

REPORT DOCUMENTATION PAGE			Form Approved OMB No. 0704-0188
<p>Public reporting burden for this collection of information is estimated to average 1 hour per response, including the time for reviewing instructions, searching existing data sources, gathering and maintaining the data needed, and completing and reviewing the collection of information. Send comments regarding this burden estimate or any other aspect of this collection of information, including suggestions for reducing this burden, to Washington Headquarters Services, Directorate for Information Operations and Reports, 1215 Jefferson Davis Highway, Suite 1204, Arlington, VA 22202-4302, and to the Office of Management and Budget, Paperwork Reduction Project (0704-0188), Washington, DC 20503.</p>			
1. AGENCY USE ONLY (Leave blank).	2. REPORT DATE	3. REPORT TYPE AND DATES COVERED	
	22 October 1996	Final Technical Report 1 Jun 93 to 31 May 96	
4. TITLE AND SUBTITLE	AASERT-92 Experimental Verification of Optimally Designed Metal Forming Processes		5. FUNDING NUMBERS F49620-93-1-0313
6. AUTHOR(S)	Ramana V. Grandhi		
7. PERFORMING ORGANIZATION NAME(S) AND ADDRESS(ES)	Department of Mechanical and Materials Engineering Wright State University Dayton, Oh 45435		8. PERFORMING ORGANIZATION REPORT NUMBER
9. SPONSORING/MONITORING AGENCY NAME(S) AND ADDRESS(ES)	AFOSR/NA 110 Duncan Avenue, Suite B 115 Boling AFB, DC 20332-8050		10. SPONSORING/MONITORING AGENCY REPORT NUMBER F49620-93-1-0313
11. SUPPLEMENTARY NOTES			
12a. DISTRIBUTION AVAILABILITY STATEMENT Approved for Public Release; Distribution Unlimited.		12b. DISTRIBUTION CODE	
<p>13. ABSTRACT (Maximum 200 words)</p> <p>This research focuses on developing a method for the preform design engineering of material forming processes. In this research, a sensitivity analysis method for preform die shape design in material forming processes is developed using the rigid visco-plastic finite element method. The preform die shapes are represented by cubic B-spline curves. The control points or coefficients of B-spline are used as the design variables. The optimization problem is to minimize the zone where the realized and desired final forging shapes do not coincide. The sensitivities of the objective function, nodal coordinates, and nodal velocities with respect to the design variables are developed in detail. A procedure for computing the sensitivities of history-dependent functions is presented. The remeshing procedure and the interpolation/transfer of the history-dependent parameters, such as effective strain, are stated. The procedures of sensitivity analysis based preform die design are also described. In addition, a method for the adjustment of the volume loss resulting from the finite element analysis is given in order to make the workpiece volume consistent in each optimization iteration. The method developed in this report is used to design the preform die shape of H-shaped forging processes, including plane strain and axisymmetric deformations. The results show that a flashless forging with a complete die fill is realized using the optimized preform die shape.</p>			
14. SUBJECT TERMS		15. NUMBER OF PAGES	
		16. PRICE CODE	
17. SECURITY CLASSIFICATION OF REPORT Unclassified	18. SECURITY CLASSIFICATION OF THIS PAGE Unclassified	19. SECURITY CLASSIFICATION OF ABSTRACT Unclassified	20. LIMITATION OF ABSTRACT UL

**AASERT-92 Experimental Verification of Optimally
Designed Metal Forming Processes**

Final Report

F49620-92-1-0313

3

Submitted by:

Ramana V. Grandhi
Department of Mechanical and Materials Engineering
Wright State University
Dayton, Oh 45435

Program Manager

Dr. Alan H. Rosenstein
AFOSR/NC
110 Duncan Ave., Suite B115
Bolling AFB, DC 20332-0001

19971006 100

Foreword

Under the AASERT program, the following graduate students were supported during the last academic year.

Mr. Ed Wright
Mr. Richard K. Huff
Miss Alicia R. Hutter



RESEARCH OBJECTIVES

This research focuses on developing a method for the preform design engineering of material forming processes. In this research, a sensitivity analysis method for preform die shape design in material forming processes is developed using the rigid visco-plastic finite element method. The preform die shapes are represented by cubic B-spline curves. The control points or coefficients of B-spline are used as the design variables. The optimization problem is to minimize the zone where the realized and desired final forging shapes do not coincide. The sensitivities of the objective function, nodal coordinates, and nodal velocities with respect to the design variables are developed in detail. A procedure for computing the sensitivities of history-dependent functions is presented. The remeshing procedure and the interpolation/transfer of the history-dependent parameters, such as effective strain, are stated. The procedures of sensitivity analysis based preform die design are also described. In addition, a method for the adjustment of the volume loss resulting from the finite element analysis is given in order to make the workpiece volume consistent in each optimization iteration. The method developed in this report is used to design the preform die shape of H-shaped forging processes, including plane strain and axisymmetric deformations. The results show that a flashless forging with a complete die fill is realized using the optimized preform die shape.

INTRODUCTION

In metal forming processes, net-shape manufacturing depends on the exactness of the die design to a large extent, especially the preform die shape design. Preform die shape design engineering includes preform die and process sequence designs. They are the most important steps for the quality control of products, material savings, and reduction of the die design/manufacture cost. Engineering experience and intuition have been the primary tools in the forging industry for determining the number of stages and the preform die shapes. Metal forming simulations using finite elements have brought opportunity for development of new methods for process sequence designs.

Kobayashi et al. [1] introduced a finite element method that simulated the metal forming processes in reverse. The process known as backward tracing was applied to several practical forging problems [2,3,4]. Han et al. [5] applied an optimization method in back-tracing. Their method determined which nodes to detach from the dies based on nodal velocities resulting from minimizing the difference between the maximum effective strain rate and the average effective strain rate for the entire billet domain. The optimization sequence is implemented in each incremental step. Zhao et al. [6,7] established a detachment criterion for backward simulation and the related preform design according to forging shape complexity control and applied this method in preform design of axisymmetric deformation problems. Zhao et al. [8] also gave an inverse die contact tracking method for designing the preform shape. The procedure starts with the forward simulation of a candidate preform shape into the final forging shape. A record of the boundary condition changes is produced by identifying when a particular die segment makes contact with the workpiece surface. This recorded boundary condition change is then modified according to the material flow characteristics. The modified boundary condition is finally used as the control criterion for node detachment during the inverse deformation simulation.

All the above methods use both forward and backward simulations and relied on selecting the appropriate detachment criteria of boundary nodes during the backward simulation. In each case, the design objectives were the preform or intermediate forging shapes rather than directly designing the dies. So the preform die shape then had to be designed to produce the preform shape of the workpiece.

Badrinarayanan and Zabaras [9, 10] developed a sensitivity analysis method for large deformation of hyperelastic viscoplastic solids that can be applied to preform design problems in metal forming. Like the backward tracing, this method designs the preform or intermediate shape of the workpiece instead of preform dies. Their method was applied to an axisymmetric disk upsetting problem where the preform is designed such that, a final forging with a minimum barreling effect is achieved. The desired results were achieved, however the axisymmetric preform shape had a concave lateral shape that is very difficult-to-forgo.

Fourment et al. [11] described a method to design the preform tools and the preform shapes. The distance between the achieved and required part is used as the objective function to be minimized. The shapes are discretized using spline functions. The design variables of the optimization problem are the displacements of the selected characteristic points of the spline in the normal direction. The gradients are calculated analytically where the friction on the tool-workpiece interface is considered as an exponential function of the sliding velocity. Shape optimization for both one and two step forging operations was performed using this method.

This project focuses on optimal design of the preform die shapes instead of the preform shapes. An optimization method for preform die shape design in metal forming is developed using forward simulation only. The preform die shapes are represented using piecewise cubic B-splines function. The objective is to reduce the zone where the actual final forging shape and desired final forging shape do not coincide. B-spline coefficients are considered as the design variables for the sensitivity analysis and optimization problem. After completing the sensitivity analysis, the optimization step is performed at the end of simulation for the selected spline coefficients. The updated spline coefficients define the new preform die shapes and a complete forging simulation is again carried out to evaluate the sensitivity and objective function. This preform die shape updating procedure is continued until no further improvement is achieved. By minimizing the objective function, the net-shape manufacturing of the final forging can be realized using the designed preform die shapes. The required sensitivity analysis for rigid-plastic or visco-rigid plastic deformation problems is developed in detail, including the velocity boundary conditions for the contact problem. The friction boundary condition at the die-workpiece interface for the sensitivity analysis is modeled by an arctangent function [1]. The remeshing procedures and volume loss adjustment are also described

and examples are presented using the sensitivity analysis and optimization method.

FINITE ELEMENT EQUATIONS

In the following, the governing equilibrium equations are presented for establishing the objective function gradients. For the complete visco-plastic analysis, reference [1] is suggested.

The element strain rate vector for 2D analysis problems can be written as:

$$\dot{\epsilon} = \begin{pmatrix} \dot{\epsilon}_x \\ \dot{\epsilon}_y \\ \dot{\epsilon}_z \\ \dot{\gamma}_{xy} \end{pmatrix} = \begin{pmatrix} \partial v_x / \partial x \\ \partial v_y / \partial y \\ 0 \\ \partial v_x / \partial y + \partial v_y / \partial x \end{pmatrix} \quad \text{for plane strain} \quad (1a)$$

$$\dot{\epsilon} = \begin{pmatrix} \dot{\epsilon}_r \\ \dot{\epsilon}_z \\ \dot{\epsilon}_\theta \\ \dot{\gamma}_{rz} \end{pmatrix} = \begin{pmatrix} \partial v_r / \partial r \\ \partial v_z / \partial z \\ v_r / r \\ \partial v_z / \partial r + \partial v_r / \partial z \end{pmatrix} \quad \text{for axisymmetric deformation} \quad (1b)$$

Substituting the elemental admissible velocity field of the 4-node linear element in equations (1a) and (1b), the element strain rate vector is represented in a unified form, as

$$\dot{\epsilon} = \begin{pmatrix} \dot{\epsilon}_1 \\ \dot{\epsilon}_2 \\ \dot{\epsilon}_3 \\ \dot{\epsilon}_4 \end{pmatrix} = \begin{pmatrix} \sum E_\alpha v_1^{(\alpha)} \\ \sum H_\alpha v_2^{(\alpha)} \\ \sum P_\alpha v_3^{(\alpha)} \\ \sum (E_\alpha v_2^{(\alpha)} + H_\alpha v_1^{(\alpha)}) \end{pmatrix} \quad (2)$$

where $(v_1^{(\alpha)}, v_2^{(\alpha)})$ are the velocity components of the α th node. They correspond to v_x and v_y , respectively. The summation is over all four nodes. P_α is zero for a plane strain problem and the row of $\dot{\epsilon}_3$ is deleted for plane stress deformation. For an axisymmetric problem, v_1 and v_2 represent v_r and v_z , respectively, and P_α becomes q_α / r , where r is the radial coordinate and expressed as:

$$r = \sum_{\alpha=1}^4 q_\alpha x_\alpha \quad (3)$$

Strain rates in the finite element formulation are typically computed from

$$\dot{\epsilon} = \mathbf{B} \mathbf{V}$$

where \mathbf{B} is the element strain rate matrix and \mathbf{V} is the nodal velocity vector of the element. \mathbf{B} matrix is expressed as:

$$\mathbf{B} = \begin{pmatrix} E_1 & 0 & E_2 & 0 & E_3 & 0 & E_4 & 0 \\ 0 & H_1 & 0 & H_2 & 0 & H_3 & 0 & H_4 \\ P_1 & 0 & P_2 & 0 & P_3 & 0 & P_4 & 0 \\ H_1 & E_1 & H_2 & E_2 & H_3 & E_3 & H_4 & E_4 \end{pmatrix} \quad (4)$$

The elemental stiffness equation of the forging problem using FEM can be expressed as:

$$\mathbf{K}(\mathbf{V}, \mathbf{X})\mathbf{V} + \mathbf{F}(\mathbf{V}, \mathbf{X}) = 0 \quad (5)$$

where

$$K_{ij}(\mathbf{V}, \mathbf{X}) = \int_V \frac{\bar{\sigma}}{\dot{\varepsilon}} P_{ij} dV + Q \int_V C_i C_j dV \quad (6a)$$

$$F_i(\mathbf{V}, \mathbf{X}) = \int_{S_C} m k \frac{2}{\pi} q_i \tan^{-1} \left(\frac{q_j u_{sj}}{u_0} \right) dS \quad (6b)$$

where \mathbf{K} is the material and process dependent nonlinear stiffness matrix, \mathbf{F} is the applied nodal point force vector. \mathbf{X} is the nodal coordinate vector of the element. Q is a large positive constant which penalizes the dilatational strain in the rigid-plastic formulation. q_j are the element shape functions expressed in the natural coordinate system (ξ, η) . $\bar{\sigma}$ is the effective stress. $\bar{\sigma} = \bar{\sigma}(\dot{\varepsilon})$ and $\bar{\sigma} = \bar{\sigma}(\dot{\varepsilon}, \dot{\varepsilon})$ for rigid-plastic and rigid-viscoplastic materials, respectively. $\dot{\varepsilon}$ is the effective strain rate. The friction on the interface between the workpiece and dies is modelled using the arctangent function of the relative sliding velocity. k is the shear yield stress and m is the constant friction factor. u_{sj} is the relative sliding velocity at node j on the die-workpiece contact interface. The sliding velocity u_s is approximated using a linear shape function:

$$u_s = \sum_{j=1}^2 q_j u_{sj}$$

u_0 is a small positive number compared to u_s . The components P_{ij} , C_i of matrix \mathbf{P} and vector \mathbf{C} are constructed by using the strain rate matrix \mathbf{B} as follows:

$$P_{ij} = B_{ki} D_{kn} B_{nj} \quad (7a)$$

$$C_i = B_{1i} + B_{2i} + B_{3i} \quad (7b)$$

$$C_j = B_{1j} + B_{2j} + B_{3j} \quad (7c)$$

where the diagonal matrix \mathbf{D} is:

$$\mathbf{D} = \begin{pmatrix} \frac{2}{3} & 0 & 0 & 0 \\ 0 & \frac{2}{3} & 0 & 0 \\ 0 & 0 & \frac{2}{3} & 0 \\ 0 & 0 & 0 & \frac{1}{3} \end{pmatrix}$$

In metal forming, the stiffness equation (5) is nonlinear. Evaluating stiffness matrices at the elemental level from equations (5) and (6), assembling them for the whole workpiece, we obtain a set of nonlinear equations. The solution is then obtained by using Newton-Raphson method which consists of linearization and application of convergence criteria.

OBJECTIVE FUNCTION AND DESIGN VARIABLES

For a two-dimensional metal forming processes, suppose that G_0 and G represent the desired shape and the actual shape of the final forging, respectively. The difference between G_0 and G is a function of the preform shape and reflects the exactness of the preform design. It is our design objective to make shape G close to G_0 by redesigning the preform dies. The objective function or difference of two shapes can be expressed as the area of the zone where the two shapes do not coincide (see figure 1).

For the discretized boundaries of the workpiece, suppose there are N boundary nodes around the achieved final shape G with coordinates (x_i, y_i) ($i = 1, 2, \dots, N$). Similarly, the boundary of the desired shape can be discretized by extending a line on the normal direction from each node on the material boundary to intersect the desired shape boundary. This provides a second set of node coordinates for the desired shape (x_{0i}, y_{0i}) ($i = 1, 2, \dots, N$). By connecting two consecutive nodes from each boundary, a quadrilateral element is formed. The four nodes of each element are locally numbered in counterclockwise direction as shown in figure 2(a) and so the area of the element can be calculated as:

$$A_j = \frac{1}{2}(x_{32}y_{12} - x_{12}y_{32}) + \frac{1}{2}(x_{14}y_{34} - x_{34}y_{14})$$

where $x_{ij} = x_i - x_j$, $y_{ij} = y_i - y_j$.

Occasionally, the actual final forging boundary will intersect the desired final forging boundary when this intersecting area occurs between two nodes. The element will appear as shown in figure 2(b). For this particular element, its area is calculated as follows:

$$A_j = \frac{1}{2}(x_{35}y_{25} - x_{25}y_{35}) + \frac{1}{2}(x_{14}y_{54} - x_{54}y_{14})$$

where (x_5, y_5) is the intersecting point.

We use the sum of the square of the subarea A_j^2 as the objective function ψ .

$$\psi = \sum_{j=1}^N A_j^2 \quad (8)$$

When ψ approaches zero, the achieved shape G will be consistent with the desired shape G_0 . Therefore, the optimization problem is to define a preforming operation that will minimize the objective function ψ .

The shapes of the preform dies for a two-dimensional model are represented using cubic B-spline functions. The B-spline shapes are controlled by varying the coefficients or the coordinates of the control points. For each control point, there are two degrees of freedom (p_{xi}, p_{yi}) $i = 1, 2, \dots, K$ for a total of $2K$ design variables. For this unconstrained problem, the BFGS algorithm [12] is used to minimize the objective function ψ with respect to the design variables p_i .

SENSITIVITY ANALYSIS

From the objective function given by equation (8), the gradient of the objective function ψ with respect to the design variable p_l is obtained as follows:

$$\frac{\partial \psi}{\partial p_l} = \sum_{i=1}^N \frac{\partial \psi}{\partial x_i} \frac{\partial x_i}{\partial p_l} + \sum_{i=1}^N \frac{\partial \psi}{\partial y_i} \frac{\partial y_i}{\partial p_l} \quad (l = 1, 2, \dots, 2K) \quad (9)$$

Differentiating the cost function ψ with respect to the coordinates x_i and y_i gives:

$$\frac{\partial \psi}{\partial x_i} = 2 \sum_{j=1}^N A_j \frac{\partial A_j}{\partial x_i}$$

$$\frac{\partial \psi}{\partial y_i} = 2 \sum_{j=1}^N A_j \frac{\partial A_j}{\partial y_i}$$

For a regular element j :

$$\frac{\partial A_j}{\partial x_1} = \frac{1}{2}(y_{34} - y_{32})$$

$$\frac{\partial A_j}{\partial y_1} = \frac{1}{2}(x_{32} - x_{34})$$

$$\frac{\partial A_j}{\partial x_2} = \frac{1}{2}(y_{32} - y_{12})$$

$$\frac{\partial A_j}{\partial y_2} = \frac{1}{2}(x_{12} - x_{32})$$

For an intersecting element j :

$$\frac{\partial A_j}{\partial x_1} = \frac{1}{2}y_{54}$$

$$\frac{\partial A_j}{\partial y_1} = -\frac{1}{2}x_{54}$$

$$\frac{\partial A_j}{\partial x_2} = -\frac{1}{2}y_{35}$$

$$\frac{\partial A_j}{\partial y_2} = \frac{1}{2}x_{35}$$

After convergence of the finite element analysis, the velocity field at the incremental simulation step is used to update the nodal coordinates using the following equation:

$$\mathbf{X}^{(t+\Delta t)} = \mathbf{X}^{(t)} + \mathbf{V}^{(t)} \Delta t \quad (10)$$

where $\mathbf{X}^{(t+\Delta t)}$ is the nodal coordinate vector at time $t+\Delta t$. $\mathbf{X}^{(t)}$ is the nodal coordinate vector at time t and $\mathbf{V}^{(t)}$ is the nodal velocity vector at time t . Differentiation of equation (10) with

respect to the design variables p_l results in

$$\frac{\partial \mathbf{X}^{(t+\Delta t)}}{\partial p_l} = \frac{\partial \mathbf{X}^{(t)}}{\partial p_l} + \frac{\partial \mathbf{V}^{(t)}}{\partial p_l} \Delta t \quad (11)$$

At the initial state ($t = 0$):

$$\frac{\partial \mathbf{X}^{(0)}}{\partial p_l} = 0 \quad (12)$$

It can be seen from equations (9) and (11) that the gradients of the objective function with respect to the design variables can be computed once the sensitivities of the nodal velocities with respect to the design variables are available.

DETERMINATION OF $\frac{\partial \mathbf{V}^{(t)}}{\partial p_l}$

The nodal velocity sensitivities $\mathbf{V}_{,p_l}$ at time t are obtained by differentiating the equilibrium equation (5) with respect to the design variable p_l at the elemental level.

$$\left(\frac{\partial \mathbf{K}}{\partial \mathbf{V}} \mathbf{V} + \mathbf{K} + \frac{\partial \mathbf{F}}{\partial \mathbf{V}} \right) \frac{\partial \mathbf{V}}{\partial p_l} = - \left(\frac{\partial \mathbf{K}}{\partial \mathbf{X}} \frac{\partial \mathbf{X}}{\partial p_l} \mathbf{V} + \frac{\partial \mathbf{F}}{\partial \mathbf{X}} \frac{\partial \mathbf{X}}{\partial p_l} \right) \quad (13a)$$

where \mathbf{X} and \mathbf{V} are the nodal coordinate and velocity vectors respectively for the element at time t .

Equation (13a) can be simply rewritten as

$$\mathbf{R} \mathbf{V}_{,p_l} = \mathbf{F}_{,p_l} \quad (13b)$$

where \mathbf{R} is the elemental stiffness matrix sensitivity (8×8), $\mathbf{F}_{,p_l}$ is the elemental force vector sensitivity and $\mathbf{V}_{,p_l}$ is the sensitivity vector of the nodal velocities with respect to the l th design variable. The components of the matrix \mathbf{R} and vector $\mathbf{F}_{,p_l}$ are expressed as follows:

$$R_{ij} = \sum_{n=1}^8 \sum_{m=1}^8 \int_V \left(\frac{1}{\dot{\varepsilon}} \frac{\partial \dot{\sigma}}{\partial \dot{\varepsilon}} - \frac{\dot{\sigma}}{\dot{\varepsilon}^2} \right) \frac{1}{\dot{\varepsilon}} P_{in} v_n v_m P_{mj} dV + K_{ij} + \frac{\partial F_i}{\partial v_j} \quad (i, j = 1, 2, \dots, 8) \quad (14a)$$

$$F_{i,p_l} = - \left(\sum_{n=1}^8 \frac{\partial F_i}{\partial x_n} \frac{\partial x_n}{\partial p_l} + \sum_{j=1}^8 \sum_{n=1}^8 \frac{\partial K_{ij}}{\partial x_n} \frac{\partial x_n}{\partial p_l} v_j \right) \quad (i = 1, 2, \dots, 8) \quad (14b)$$

After evaluating the sensitivities of the stiffness matrix and the nodal force vector at the elemental level using equations (13) and (14), they are assembled for the whole workpiece. A set of simultaneous linear algebraic equations is obtained as

$$\bar{\mathbf{R}} \bar{\mathbf{V}}_{,p_l} = \bar{\mathbf{F}}_{,p_l} \quad (15)$$

For a given initial guess of the preform die shape, the finite element analysis of the preform stage is performed. In each incremental simulation step, the sensitivities of the node velocities to the design variables are obtained by solving equation (15) after the finite element solution in this step has converged. The sensitivities of the nodal coordinates with respect to the design variables are dependent on the deformation history and so are updated using equation (11). Once the simulation of the preform stage is finished, the simulation of the final forging stage is started. During the simulation of the final stage, the sensitivities of the boundary node velocities with respect to the design variables are zero since the final die shape does not change. When the final stage simulation is finished, the resulting sensitivities of the nodal coordinates with respect to the design variables are used to calculate the objective function gradients using equation (9) and the objective function is calculated using equation (8). After a complete simulation including the preform and final stages is finished, the optimization program DOT [13] is called to provide new control point coordinates for the preform dies. Usually, no upper and lower bounds are imposed on the design variables except in particular cases such as when a control point of the preform die must be fixed if half or quarter symmetry is used in the analysis. At this point, the optimization program also checks to see if the optimality conditions are satisfied. If the optimality conditions are not satisfied, the preform die shapes are updated using the new control points and the next optimization step begins with the initial state. If the optimality conditions are satisfied with the current shapes, the design objectives are met. The design optimization flow chart for the two-stage forging process is shown in figure 3.

DETERMINATION OF $\frac{\partial K_{ij}}{\partial x_n}$, $\frac{\partial F_i}{\partial x_n}$, $\frac{\partial F_i}{\partial v_j}$

According to equations (6a) and (6b), the derivatives $\frac{\partial K_{ij}}{\partial x_n}$, $\frac{\partial F_i}{\partial x_n}$ and $\frac{\partial F_i}{\partial v_j}$ in equation (14) at the elemental level are developed as follows:

$$\frac{\partial F_i}{\partial v_j} = \int_S m k \frac{2}{\pi} q_i q_j \frac{u_0}{u_0^2 + (q_k u_{kj})^2} dS \quad (16)$$

$$\frac{\partial F_i}{\partial x_n} = \sum_{\alpha=1}^8 \sum_{k=1}^8 \int_S \frac{m}{\sqrt{3\pi}} \frac{\partial \bar{\sigma}}{\partial \bar{\epsilon}} \frac{1}{\bar{\epsilon}} q_i \frac{1}{\bar{\epsilon}} v_\alpha \frac{\partial P_{ak}}{\partial x_n} v_k \tan^{-1} \left(\frac{q_j u_{sj}}{u_0} \right) dS + \int_{S_C} m k \frac{2}{\pi} q_i \tan^{-1} \left(\frac{q_j u_{sj}}{u_0} \right) \frac{\partial (dS)}{\partial x_n} \quad (17)$$

$$\begin{aligned} \frac{\partial K_{ij}}{\partial x_n} = & \int_V \left(\frac{1}{\bar{\epsilon}} \frac{\partial \bar{\sigma}}{\partial \bar{\epsilon}} - \frac{\bar{\sigma}}{\bar{\epsilon}^2} \right) \frac{1}{2\bar{\epsilon}} \frac{\partial (\mathbf{V}^T \mathbf{P} \mathbf{V})}{\partial x_n} P_{ij} dV + \int_V \frac{\bar{\sigma}}{\bar{\epsilon}} \frac{\partial P_{ij}}{\partial x_n} dV + Q \int_V \frac{\partial C_i}{\partial x_n} C_j dV + Q \int_V C_i \frac{\partial C_j}{\partial x_n} dV \\ & + \int_V \frac{\bar{\sigma}}{\bar{\epsilon}} P_{ij} \frac{\partial (dV)}{\partial x_n} + Q \int_V C_i C_j \frac{\partial (dV)}{\partial x_n} \end{aligned} \quad (18)$$

where $\frac{\partial C_i}{\partial x_n}$, $\frac{\partial C_j}{\partial x_n}$, $\frac{\partial P_{ij}}{\partial x_n}$ and $\frac{\partial(\mathbf{V}^T \mathbf{P} \mathbf{V})}{\partial x_n}$ can be obtained according to equations (7a) through (7c).

$$\frac{\partial C_i}{\partial x_n} = \frac{\partial B_{1i}}{\partial x_n} + \frac{\partial B_{2i}}{\partial x_n} + \frac{\partial B_{3i}}{\partial x_n} \quad (19a)$$

$$\frac{\partial C_j}{\partial x_n} = \frac{\partial B_{1j}}{\partial x_n} + \frac{\partial B_{2j}}{\partial x_n} + \frac{\partial B_{3j}}{\partial x_n} \quad (19b)$$

$$\frac{\partial P_{ij}}{\partial x_n} = \sum_{k=1}^4 \sum_{m=1}^4 \left(\frac{\partial B_{ki}}{\partial x_n} D_{km} B_{mj} + B_{ki} D_{km} \frac{\partial B_{mj}}{\partial x_n} \right) \quad (19c)$$

$$\frac{\partial(\mathbf{V}^T \mathbf{P} \mathbf{V})}{\partial x_n} = \sum_{m=1}^8 \sum_{k=1}^8 v_m \frac{\partial P_{mk}}{\partial x_n} v_k \quad (19d)$$

The derivative matrix $\frac{\partial \mathbf{B}}{\partial \mathbf{X}}$ can be obtained by calculating $\frac{\partial E_i}{\partial x_j}$, $\frac{\partial H_i}{\partial y_j}$, $\frac{\partial E_i}{\partial y_j}$, $\frac{\partial H_i}{\partial x_j}$ from the \mathbf{B} matrix given by equation (4). The components of $\frac{\partial \mathbf{B}}{\partial \mathbf{X}}$ are expressed as follows:

$$\frac{\partial E_i}{\partial x_j} = -E_i E_j \quad (i, j = 1, 2, 3, 4)$$

$$\frac{\partial H_i}{\partial y_j} = -H_i H_j \quad (i, j = 1, 2, 3, 4)$$

$$\frac{\partial E_i}{\partial y_j} = A_{ij}/8|\mathbf{J}| - E_i H_j \quad (i, j = 1, 2, 3, 4)$$

$$\frac{\partial H_i}{\partial x_j} = -A_{ij}/8|\mathbf{J}| - H_i E_j \quad (i, j = 1, 2, 3, 4)$$

$$\frac{\partial P_i}{\partial x_j} = -q_i q_j / r^2 \quad (i, j = 1, 2, 3, 4)$$

$$\frac{\partial P_i}{\partial y_j} = 0 \quad (i, j = 1, 2, 3, 4)$$

where $|\mathbf{J}|$ is the determinant of Jacobian matrix and expressed as:

$$|\mathbf{J}| = \frac{1}{8} [(x_{13}y_{24} - x_{24}y_{13}) + (x_{34}y_{12} - x_{12}y_{34})\xi + (x_{23}y_{14} - x_{14}y_{23})\eta] \quad (20)$$

where $x_{ij} = x_i - x_j$, $y_{ij} = y_i - y_j$ ($i, j = 1, 2, 3, 4$). For a plane strain problem, $\frac{\partial P_i}{\partial x_j} = \frac{\partial P_i}{\partial y_j} = 0$ ($i, j = 1, 2, 3, 4$). The coefficients A_{ij} are given by a matrix \mathbf{A}

$$\mathbf{A} = \begin{pmatrix} 0 & \eta - 1 & \xi - \eta & 1 - \xi \\ 1 - \eta & 0 & -(1 + \xi) & \xi + \eta \\ \eta - \xi & 1 + \xi & 0 & -(1 + \eta) \\ \xi - 1 & -(\xi + \eta) & 1 + \eta & 0 \end{pmatrix}$$

Interestingly, the coefficient matrix \mathbf{A} is an antisymmetric matrix because $\mathbf{A}^T = -\mathbf{A}$.

It should be noted that the differential volume dV and area dS are also dependant on the nodal coordinate vector \mathbf{X} . By using the natural coordinates ($-1 \leq \xi \leq 1, -1 \leq \eta \leq 1$) in the two-dimensional space, $\frac{\partial(dS)}{\partial x_n}$ and $\frac{\partial(dV)}{\partial x_n}$ can be represented as follows.

For a plane strain problem:

$$\frac{\partial(dS)}{\partial x_n} = \frac{\partial|\mathbf{J}_s|}{\partial x_n} d\xi$$

$$\frac{\partial(dV)}{\partial x_n} = \frac{\partial|\mathbf{J}_s|}{\partial x_n} d\xi d\eta$$

where $|\mathbf{J}_s|$ is the determinant of the Jacobian of the coordinate transformation matrix on the die-workpiece interface.

$$|\mathbf{J}_s| = \frac{1}{2} \sqrt{(x_1 - x_2)^2 + (y_1 - y_2)^2} \quad (21)$$

where (x_1, y_1) and (x_2, y_2) are the coordinates of the two nodes of the element in contact with the die surface.

For an axisymmetric problem:

$$\begin{aligned} \frac{\partial(dS)}{\partial x_n} &= \frac{\partial(r|\mathbf{J}_s|)}{\partial x_n} d\xi = (|\mathbf{J}_s| \frac{\partial r}{\partial x_n} + r \frac{\partial|\mathbf{J}_s|}{\partial x_n}) d\xi \\ \frac{\partial(dV)}{\partial x_n} &= \frac{\partial(r|\mathbf{J}|)}{\partial x_n} d\xi d\eta = (|\mathbf{J}| \frac{\partial r}{\partial x_n} + r \frac{\partial|\mathbf{J}|}{\partial x_n}) d\xi d\eta \end{aligned}$$

where r is the radial position of the integration point and defined by equation (3)

$$\frac{\partial r}{\partial x_{2i-1}} = q_i \quad \frac{\partial r}{\partial x_{2i}} = 0 \quad (i = 1, 2, 3, 4)$$

$\frac{\partial|\mathbf{J}|}{\partial x_n}$ and $\frac{\partial|\mathbf{J}_s|}{\partial x_n}$ can be obtained by using equations (20) and (21), respectively.

BOUNDARY CONDITIONS

On the friction boundary, the traction is prescribed in the tangential direction and the velocity is prescribed in the normal direction to the surface. When the interface direction is inclined with respect to the global coordinate axis, the coordinate transformation of the stiffness matrix upon the inclined direction is necessary in order to impose the mixed boundary conditions. The local coordinate system is defined as the inclined boundary coordinate system (see figure 4). The velocity boundary conditions of the i th node in contact with the dies are:

$$\mathbf{v}_{i_n} = \mathbf{V}_{die}^T \cdot \mathbf{n} = (v_{die_x}, v_{die_y}) \begin{pmatrix} -\sin\beta \\ \cos\beta \end{pmatrix} \quad (22)$$

where v_{i_n} is the velocity component of the node i in the normal direction of the interface surface. \mathbf{V}_{die} is the die velocity vector. \mathbf{n} is the unit normal on the interface surface. β is measured from the x axis in the global coordinate system to the x' axis of the local coordinate system in counterclockwise direction. For a B-spline function defined by $y = y(p_i, x)$

($l = 1, 2, \dots, 2K$), the slope of the B-spline curve is $\frac{dy}{dx} = y_x = \tan\beta$. Thus, the following relations are obtained

$$\sin\beta = \frac{y_x}{\sqrt{1 + y_x^2}}$$

$$\cos\beta = \frac{1}{\sqrt{1 + y_x^2}}$$

Differentiating equation (22) with respect to the design variable p_l gives the following relationship:

$$\frac{\partial v_{in}}{\partial p_l} = \mathbf{V}_{die}^T \frac{\partial \mathbf{n}}{\partial p_l} = -v_{die_x} \frac{\partial \sin\beta}{\partial p_l} + v_{die_y} \frac{\partial \cos\beta}{\partial p_l} \quad (23)$$

where $\frac{\partial \mathbf{n}}{\partial p_l}$ is the sensitivity of the normal of the die surface to the design variable p_l . It can be obtained by differentiating the equation which defines the normal of the B-spline curve.

$$\frac{\partial \mathbf{n}}{\partial p_l} = \left(\begin{array}{c} -\frac{\partial \sin\beta}{\partial p_l} \\ \frac{\partial \cos\beta}{\partial p_l} \end{array} \right) = \left(\begin{array}{c} -\frac{y_{xp_l}}{(1+y_x^2)^{3/2}} \\ -\frac{y_{xp_l} y_x}{(1+y_x^2)^{3/2}} \end{array} \right) \quad (24)$$

where $y_{xp_l} = \frac{\partial y_x}{\partial p_l}$. If the node i is not in contact with part of the dies that is being optimized, or if the dies are not optimized (for instance, during the final stage forging), then $\frac{\partial \mathbf{n}}{\partial p_l} = 0$.

Usually, v_{die_x} is equal to zero. So equation (23) can be simplified into

$$\frac{\partial v_{in}}{\partial p_l} = v_{die_y} \frac{\partial \cos\beta}{\partial p_l} \quad (25)$$

The above boundary conditions should be imposed in the local coordinate system and the sensitivity equations (15) are solved in the local coordinate system. When the solution is obtained, it is transformed back to the global coordinate system.

CUBIC B-SPLINE AND ITS DIFFERENTIATION

Given the control points (p_{xi}, p_{yi}) ($i = 1, 2, \dots, K$), the design variables are $\mathbf{p} = (p_1, p_2, \dots, p_{2K}) = (p_{x1}, p_{y1}, \dots, p_{xK}, p_{yK})$. The (x, y) coordinates of the i th piecewise cubic B-spline function can be expressed by a parametric function as [14]

$$x = \frac{1}{6}[(1-s)^3 p_{xi} + (4-6s^2+3s^3)p_{xi+1} + (1+3s+3s^2-3s^3)p_{xi+2} + s^3 p_{xi+3}] \quad (26a)$$

$$y = \frac{1}{6}[(1-s)^3 p_{yi} + (4-6s^2+3s^3)p_{yi+1} + (1+3s+3s^2-3s^3)p_{yi+2} + s^3 p_{yi+3}] \quad (26b)$$

where $0 \leq s \leq 1$.

Differentiation of the B-spline, y_x can be obtained using the following equation:

$$y_x = \frac{dy}{dx} = \frac{\partial y}{\partial s} / \frac{\partial x}{\partial s} \quad (27)$$

where

$$\frac{\partial y}{\partial s} = \frac{1}{2} [-(1-s)^2 p_{y_i} + (-4s+3s^2) p_{y_{i+1}} + (1+2s-3s^2) p_{y_{i+2}} + s^2 p_{y_{i+3}}] \quad (28a)$$

$$\frac{\partial x}{\partial s} = \frac{1}{2} [-(1-s)^2 P_{x_i} + (-4s+3s^2) p_{x_{i+1}} + (1+2s-3s^2) p_{x_{i+2}} + s^2 p_{x_{i+3}}] \quad (28b)$$

The differentiations of the slope of B-spline to the design variables or control points (p_{x_i}, p_{y_i}) are as follows:

$$\frac{\partial^2 y}{\partial x \partial p_{y_i}} = -\frac{(1-s)^2}{2 \frac{\partial x}{\partial s}} \quad (29a)$$

$$\frac{\partial^2 y}{\partial x \partial p_{y_{i+1}}} = \frac{-4s+3s^2}{2 \frac{\partial x}{\partial s}} \quad (29b)$$

$$\frac{\partial^2 y}{\partial x \partial p_{y_{i+2}}} = \frac{1+2s-3s^2}{2 \frac{\partial x}{\partial s}} \quad (29c)$$

$$\frac{\partial^2 y}{\partial x \partial p_{y_{i+3}}} = \frac{s^2}{2 \frac{\partial x}{\partial s}} \quad (29d)$$

$$\frac{\partial^2 y}{\partial x \partial p_{x_i}} = \frac{(1-s)^2}{2(\frac{\partial x}{\partial s})^2} \frac{\partial y}{\partial s} \quad (30a)$$

$$\frac{\partial^2 y}{\partial x \partial p_{x_{i+1}}} = -\frac{-4s+3s^2}{2(\frac{\partial x}{\partial s})^2} \frac{\partial y}{\partial s} \quad (30b)$$

$$\frac{\partial^2 y}{\partial x \partial p_{x_{i+2}}} = -\frac{1+2s-3s^2}{2(\frac{\partial x}{\partial s})^2} \frac{\partial y}{\partial s} \quad (30c)$$

$$\frac{\partial^2 y}{\partial x \partial p_{x_{i+3}}} = -\frac{s^2}{2(\frac{\partial x}{\partial s})^2} \frac{\partial y}{\partial s} \quad (30d)$$

Substituting y_x (equations (27) and (28)) and $y_{x_{p_i}}$ (equations (29) and (30)) in equation (24), $\frac{\partial n}{\partial p_i}$ is solved. Then substituting equation (24) in equation (23) or (25) gives the velocity boundary conditions for the sensitivity analysis.

REMESHING

In practical forming processes, large deformations eventually lead to indeterminant elements when the determinant of Jacobian matrix becomes negative. Therefore, a new mesh of the workpiece must be defined and the history-dependant variables must be transferred to the new mesh system. The history-dependant field variables are effective strains, node temperatures (only for non-isothermal analysis) and the sensitivities of the node coordinates with respect to the design variables. These values must be defined on the new mesh by interpolation.

Sensitivities of the node coordinates with respect to the design variables are given at the

node points. Thus, it is assumed that the distributions of node coordinate sensitivities within the workpiece domain can be expressed by using the element shape functions. Interpolation is done by evaluating the sensitivities at the new node locations.

ADJUSTMENT OF VOLUME LOSS

A small volume loss of the workpiece due to geometry update within a finite time-increment is inevitable. In addition, the amount of volume loss will vary due to remeshing. Limiting the volume loss within a small percentage of the total deforming volume is a major consideration in the prediction of proper die fill and defect formation, which are important in process design. In a conventional finite element simulation, the amount of volume loss is controlled by limiting the maximum allowable time-increment.

The initial billet volume is determined to be equal to the final forging volume. However, with volume loss, the achieved final forging volume V is always smaller than the initial billet volume V_0 . The objective function depends on the area of the zone where two final forging shapes do not coincide. Therefore, the objective function is affected adversely by the volume loss. More importantly, the magnitude of volume loss may vary from one optimization iteration to another. This results in convergence problems of the optimization algorithm.

To support design optimization, a volume loss adjustment procedure is incorporated in the simulation process. After each time-increment, the y-coordinates of the nodes in contact with the die surfaces are adjusted to ensure the workpiece volume equal to the initial volume V_0 . At the same time, the die position is also adjusted by the same distance.

Figure 5 shows an element in contact with the upper die. Suppose that the coordinates of node 4 are (x_4, y_4) and coordinate adjustment amount in y-direction is Δy . The new coordinates of node 4 are $(x_4, y_4 + \Delta y)$. For axisymmetric problems, the volume of the element $\overline{1234}$ is:

$$V_e = \frac{1}{2}C_1(x_{32}y_{12} - x_{12}y_{32}) + \frac{1}{2}C_2(x_{14}y_{34} - x_{34}y_{14})$$

where $C_1 = \frac{2\pi}{3}(x_1 + x_2 + x_3)$, $C_2 = \frac{2\pi}{3}(x_1 + x_3 + x_4)$. For plane strain problems, $C_1 = C_2 = 1$.

The volume of the element $\overline{1234'}$ is:

$$V'_e = \frac{1}{2}C_1(x_{32}y_{12} - x_{12}y_{32}) + \frac{1}{2}C_2(x_{14}y_{34'} - x_{34}y_{14'})$$

The volume increase due to the adjustment of the node 4 is:

$$\Delta V_4 = V'_e - V_e = \frac{1}{2}C_2(x_{34} - x_{14}) \cdot \Delta y = S_4 \cdot \Delta y$$

By accumulating the volume increase due to the nodal coordinate adjustment over all the nodes in contact with the dies, the total volume increase ΔV_T is obtained.

$$\Delta V_T = \Delta y \sum S_i$$

Letting the total volume increase due to the nodal coordinate adjustment equal to the volume loss ($V_0 - V$) resulting from finite element analysis, we obtain a factor for adjusting the y-coordinates of the nodes in contact with the dies.

$$\Delta y = \frac{\Delta V_T}{\sum S_i} = \frac{V_0 - V}{\sum S_i}$$

Numerical analysis examples show that the adjustment amount Δy for volume loss in each time-increment step is very small. Usually the ratio of Δy to the time-increment is about $0.001 \sim 0.0001$. Such a small adjustment does not affect the material flow patterns. But after the adjustment, the volume constancy is realized in every time-increment step. The final forging volume is exactly equal to the initial volume in various optimization iterations and the convergence of optimization is improved significantly.

DESIGN EXAMPLES

The sensitivity analysis presented here are used to design the preform die shape of H-shaped forging in both plane strain and axisymmetric deformation modes. The goal is to design the preform die shape such that, after the final forging stage, a flashless forging with a complete die fill is obtained.

In each case, the forging process is isothermal. A non-strain hardening material having the constitutive relation $\bar{\sigma} = Y_0 \dot{\varepsilon}^{0.145}$ with $Y_0 = 33.99 \text{ MPa}$ was used in this example. A constant shear friction factor was assumed between the workpiece and the dies. The lower die is stationary and the upper die velocity is -1.0 mm/s . Since the forging is symmetric about the vertical and horizontal axes, only one quarter of the cross section is considered for the finite element analysis. The selection of the total number of control points representing the preform die shapes depends on the complexity of the final die shapes. If the final die shapes are complex, more control points should be used. However, additional control points need more computation time. In this example, ten control points (p_{x_i}, p_{y_i}) ($p_{x_1} > p_{x_2} > \dots > p_{x_{10}}$) were used to represent the preform die shape. Therefore, there are seven spline pieces with twenty design variables p_l ($l = 1, 2, \dots, 20$). Phantom control points are assigned at the end points of the preform die $p_{x_3} = -p_{x_1} = b$ and $p_{x_2} = 0$ since the splines do not interpolate to the end points. Therefore, side constraints are imposed on design variables p_{x_1}, p_{x_2} and p_{x_3} during the optimization.

PLANE STRAIN DEFORMATION

In this case, the initial guess of the preform die shape is a flat die. The constant shear friction factor m is taken as 0.2. The height of the preform shape at vertical symmetry axis ($z = 0$) is kept same for each optimization iteration. This height determines the stroke of the preforming stage. Figure 6 shows the resulting preform shapes and corresponding final forging shapes at various optimization iterations. Figure 7 shows the comparison of the three final forging shapes. It can be seen that the optimized shape is almost same as the desired shape. Figure 8 shows the objective function history over the optimization process. Using the flat die initially gives a final forging with flash and incomplete die fill. After four

optimization iterations, the die cavity is completely filled and a flashless final forging is obtained. The objective function value is reduced to $0.178mm^4$ compared to a starting value of $17.096mm^4$. For the fifth iteration, the preform die has a relatively deep cavity which can also give a flashless final forging shape but the objective function has increased slightly. This is due to elements overlapping the curved die surface. This situation can be resolved by using a finer mesh. From the fifth iteration on, the objective function changes very little. Therefore, the preform die shape at either the fourth or seventh iteration can be selected as the optimal die shape. Figure 9 shows how the preform die shapes evolve with each optimization step.

AXISYMMETRIC DEFORMATION

In this case, the desired final forging shape cross section, friction factor m and initial guess of the preform die shape are same as those in plane strain deformation. The mesh deformation patterns at the end of the preforming and final forging stages at each optimization iteration are shown in figure 10. Figure 11 shows the comparison of the three final forging shapes. The optimized shape is close enough to the desired shape. The optimization iteration history is shown in figure 12. Similar to the previous case, for the initial flat preform die, the achieved final forging has a flash although it is small and the final die cavity is not completely filled. The forging shape does not satisfy the dimensional requirement. After five design iterations, the final die cavity is completely filled and a flashless final forging is obtained. The objective function is reduced from $9.309mm^4$ to $0.210mm^4$. In this case, remeshing was needed. The preform die shape iteration history for axisymmetric problem is shown in figure 13. From these two analysis cases, it can be concluded that the numerical optimization method developed in this work is very effective in realizing a net-shape forging process.

The optimization method and related sensitivity analysis presented in this work have been incorporated into a finite element code developed specifically for analyzing metal forming processes. It should be emphasized that, in fact, the experimental verification of the preform die shape design method developed in this work is equivalent to the verification of the finite element code. Once a preform die shape is obtained from an optimization iteration, the finite element analysis is performed to see the material flow and the workpiece shape at

the end of preforming and final forging stages. Therefore, the finite element analysis verifies the preform die design in every optimization iteration until the achieved shape is close enough to the desired shape. The results from the finite element code used in this report were found to correlate well with the commercial code ANTARES [15]. It was also validated for forging, rolling and extrusion simulations and experiments. The comparison, validation and experiment show that the finite element code is reliable. Consequently, the results of preform die shape design in this work are reasonable.

CONCLUSIONS

An optimization and sensitivity analysis methods for preform die shape design in realizing net-shape final forging processes was developed. The method includes the determination of the objective function, sensitivity analysis and the velocity boundary conditions. The optimization procedures, remeshing and the adjustment of volume loss due to finite element analysis were also introduced. The sensitivity of the objective function is calculated by the accumulated sensitivity of the nodal coordinates to the design variables throughout an entire simulation including the preforming and final forging processes. The method was applied to design the preform die shape in H-shaped forging processes, including plane strain and axisymmetric deformations. The preform shapes were obtained from the preforming stage using optimized preform die shapes. After the final stage forging, a flashless forging with complete die fill was produced. The design results are consistent with the desired final shapes. This procedure indicates that the computed sensitivity fields and the results of the preform die design are satisfactory. Each optimization step required just one complete forging simulation and the procedure is very efficient. The method is very effective in realizing a net-shape forging. Future research needs to include the optimization of other important aspects, such as uniform deformation and energy requirement, so as to realize multi-objective optimization design of metal forming processes.

This research strictly addresses the preform die shape design. The initial billet stock size (aspect ratio) is assumed empirically. The different stock size would result in different preform die shapes. So optimization of starting stock size has become a topic for future research. This could be incorporated by one additional design variable, say height for example, since the required volume is known. The method of computing shape sensitivity for this design variable need to be derived and implemented in a manner that is valid for both single and multi-stage operations.

This research concentrates on the preform die shape of the two-dimensional problems. The method and ideas can also be applied to the preform die shape design for three-dimensional problems. The objective function can be expressed as the volume of the zone where the desired and actually achieved shapes do not coincide. The preform die shapes are modeled using surface splines. The control points of the surface splines are used as the

design variables. For three-dimensional problems, the computer time may become the major concern due to a large number of elements and design variables.

REFERENCES

1. S. Kobayashi, S. I. Oh and T. Altan, *Metal Forming and the Finite Element Method*, Oxford University Press, New York (1989).
2. N. Kim and S. Kobayashi, 'Preform Design in H-shaped Cross Section Axisymmetric Forging by Finite Element Method', *International Journal of Machine Tools & Manufacture*, **30**, 243-268 (1990).
3. B. S. Kang, N. Kim and S. Kobayashi, 'Computer-Aided Preform Design in Forging of An Airfoil Section Blade', *International Journal of Machine Tools & Manufacture*, **30**, 43-52 (1990).
4. B. S. Kang and S. Kobayashi, 'Preform Design in Rolling Processes by the Three Dimensional Finite Element Method', *International Journal of Machine Tools & Manufacture*, **31**, 139-151 (1991).
5. C. S. Han, R. V. Grandhi and R. Srinivasan, 'Optimum Design of Forging Die Shapes Using Nonlinear Finite Element Analysis', *AIAA Journal*, **31**, 774-781 (1993).
6. G. Zhao, E. Wright and R.V. Grandhi, 'Preform Design in Forging Processes Using Non-linear Finite Element Method', *Transactions of NAMRI/SME*, **22**, 17-24 (1994).
7. G. Zhao, E. Wright and R. V. Grandhi, 'Forging Preform Design With Shape Complexity Control in Simulating Backward Deformation', *International Journal of Machine Tools & Manufacture*, **35**, 1225-1239 (1995).
8. G. Zhao, E. Wright and R. V. Grandhi, 'Computer Aided Preform Design in Forging Using the Inverse Die Contact Tracking Method', *International Journal of Machine Tools & Manufacture*, **36**, 755-769 (1996).
9. S. Badrinarayanan and N. Zabaras, 'Preform Design in Metal Forming', *NUMIFORM'95*, Cornell University, Ithaca, New York, USA, Edited by S. F. Shen and P. R. Dawson, Published by A.A. Balkema/Rotterdam/ brookfield, 533-538 (1995).
10. S. Badrinarayanan and N. Zabaras, 'A Sensitivity Analysis for the Design of Metal Forming Processes', *Computer Methods in Applied Mechanics and Engineering*, **129**, 319-348 (1996).

11. L. Fourment, T. Balan and J. L. Chenot, 'Shape Optimal Design in Forging', *NUMIFORM'95*, Cornell University, Ithaca, New York, USA, Edited by S. F. Shen and P. R. Dawson, Published by A.A. Balkema/Rotterdam/ Brookfield, 557-562 (1995).
12. R. Fletcher, *Practical Methods of Optimization*, John Wiley and Sons, New York (1987).
13. Vanderplaats Research & Development, Inc., *DOT Users Manual*, Colorado Springs, Colorado, Version 4.20 (1995).
14. E. V. Shikin, *Handbook on Splines for the User*, CRC Press, Boca Raton, Florida (1995).
15. UES, Inc., *ANTARES Primer Manual*, Dayton, Ohio, Version 4.0 (1995).

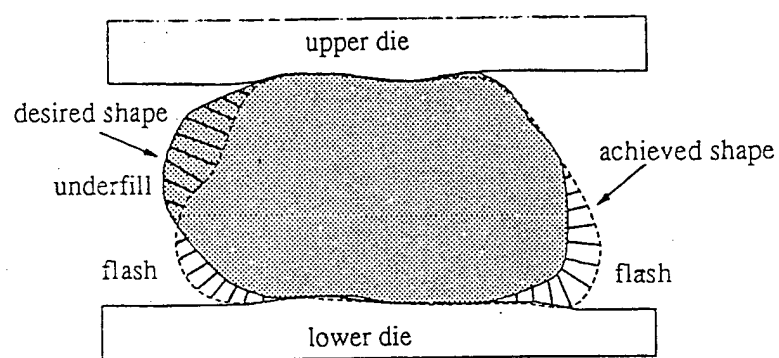


Fig 1: Desired and actually
achieved final forging shapes.

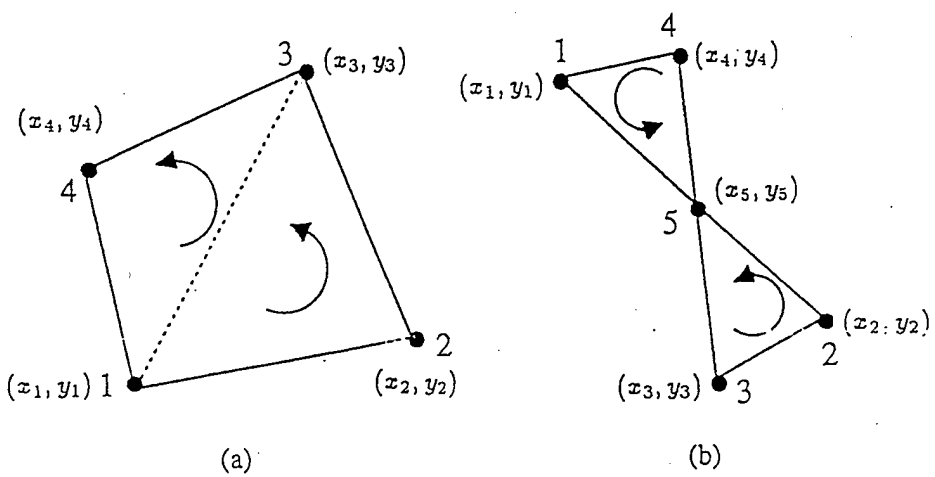


Fig 2. Elements for calculating the objective function.

(a) Regular element, (b) Intersecting element.

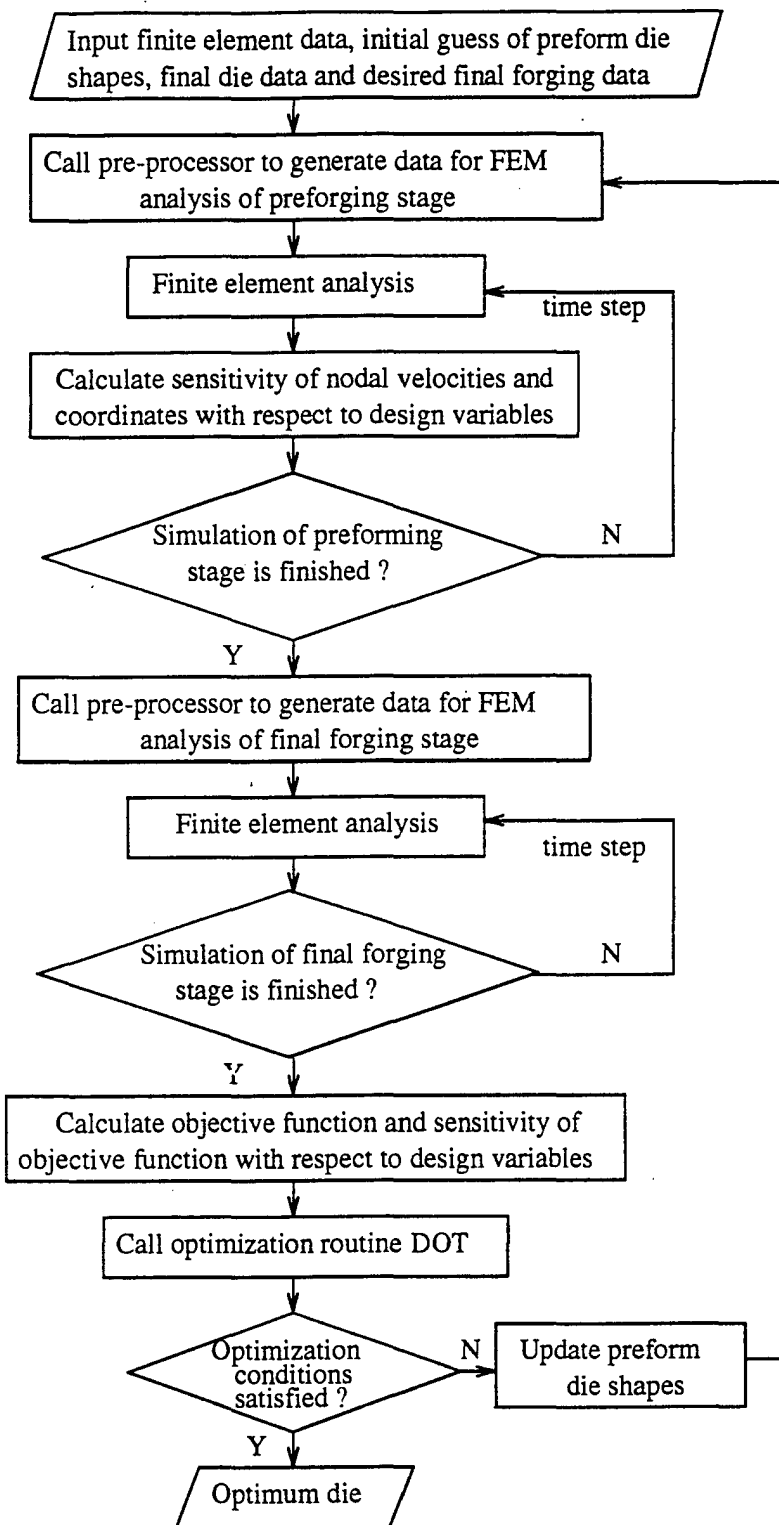


Fig 3. Sensitivity analysis based preform die shape design

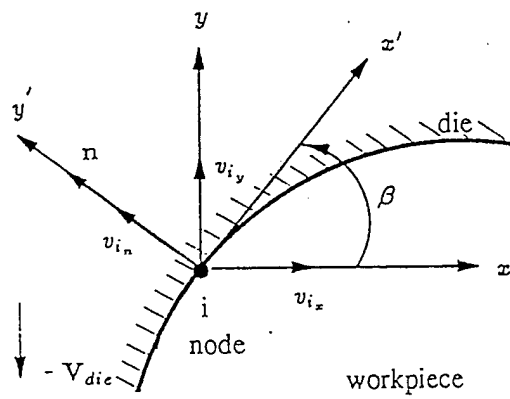


Fig 4. Velocity boundary condition
of a node in contact with die.

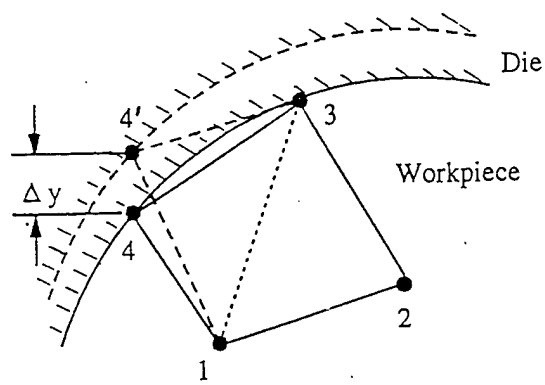


Fig 5. Adjustment of volume loss.

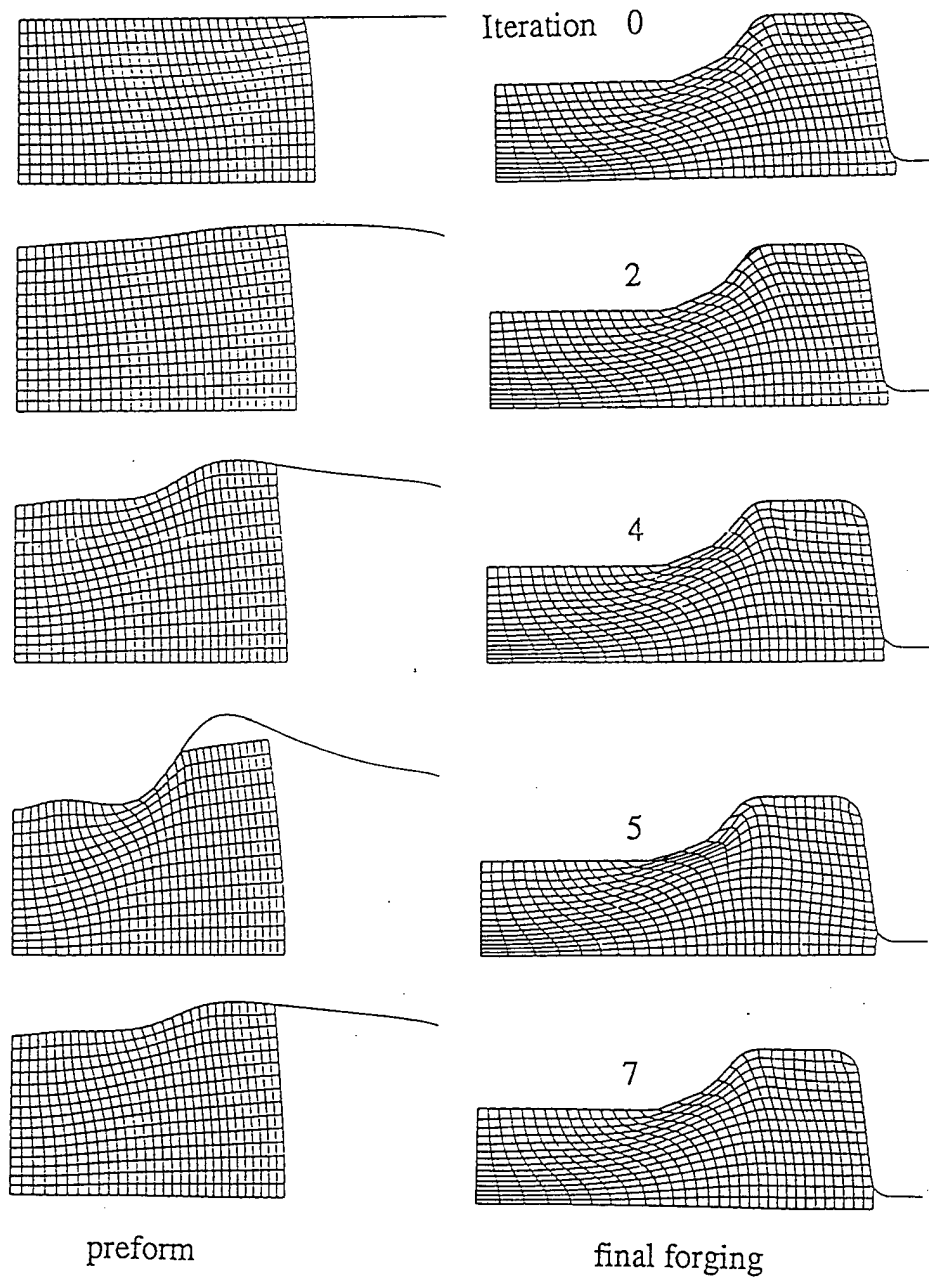


Fig 6. Preform and final forging shapes at various optimization iterations in plane strain deformation.

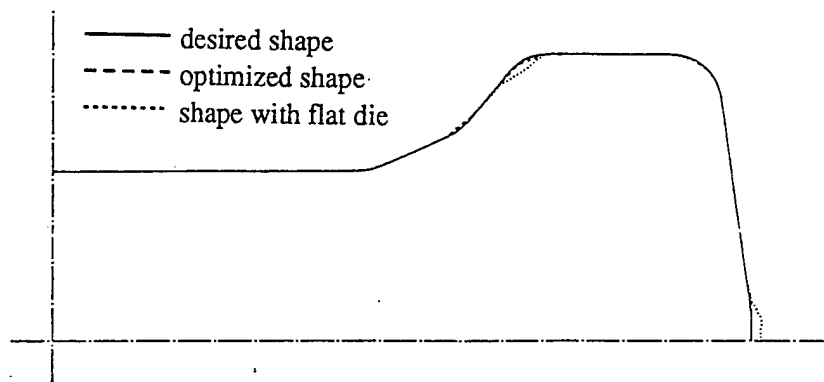


Fig 7. Comparison of the final forging shapes
in plane strain deformation.

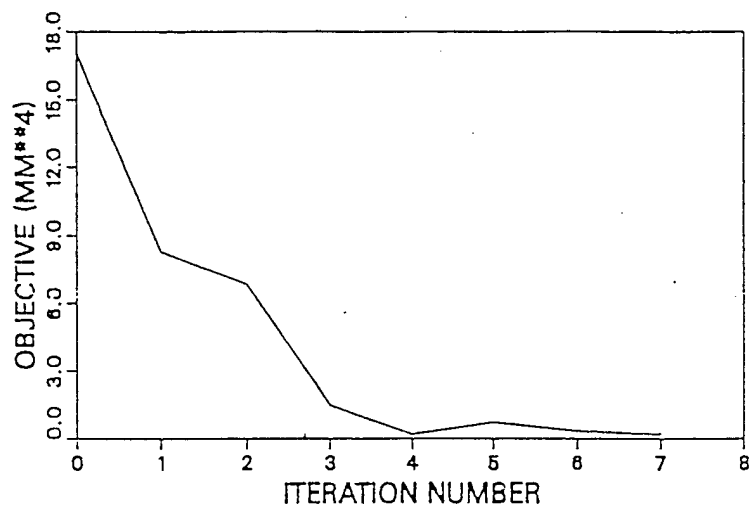


Fig 8. Objective function vs. optimization iteration in plane strain deformation.

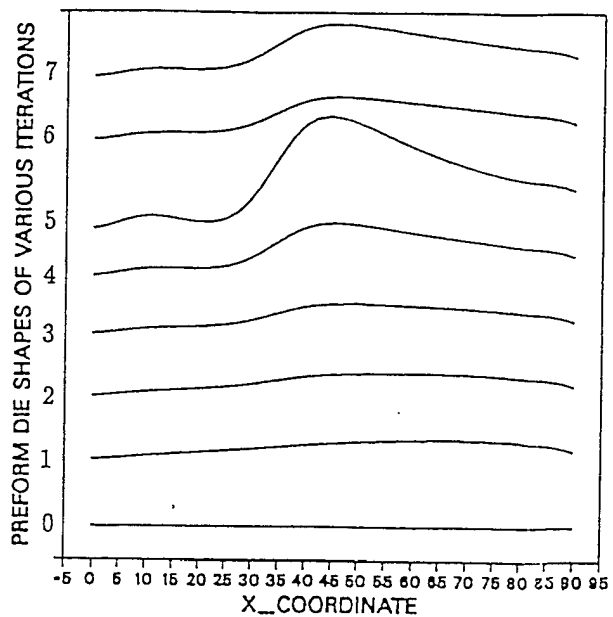


Fig 9. Iteration history of the preform die shapes in plane strain deformation.

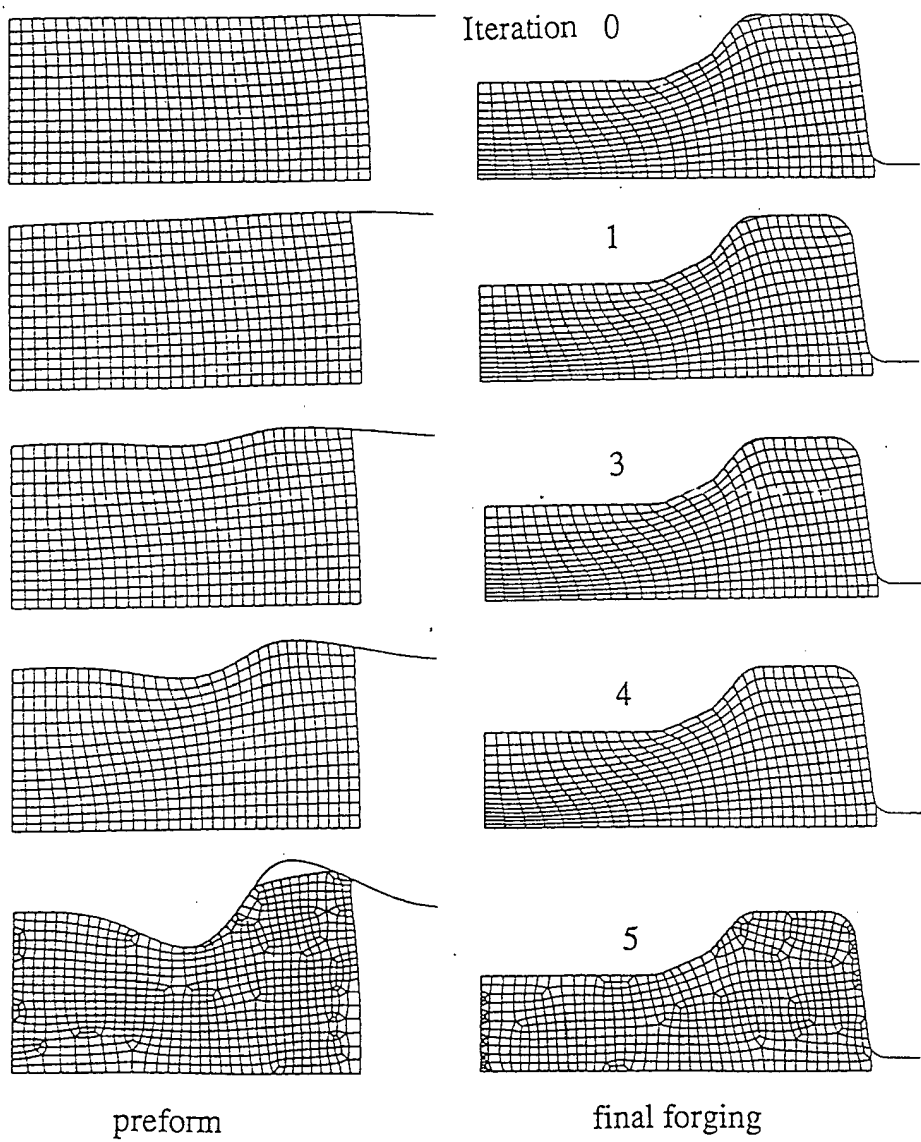


Fig 10. Preform and final forging shapes at various optimization iterations in axisymmetric deformation.

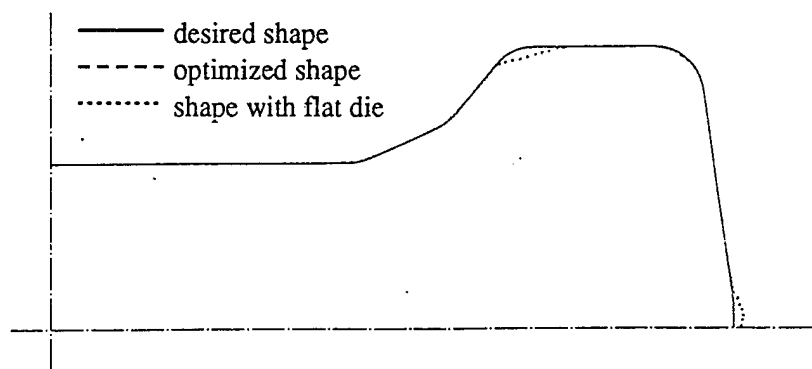


Fig 11. Comparison of the final forging shapes
in axisymmetric deformation.

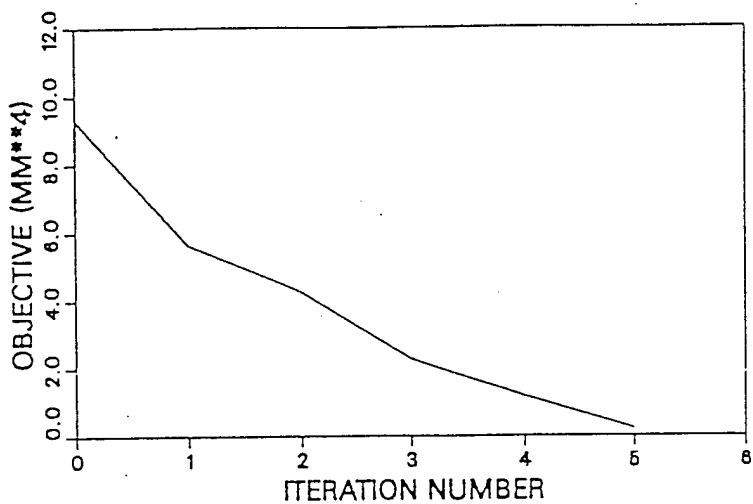


Fig 12. Objective function vs. optimization iteration in axisymmetric deformation.

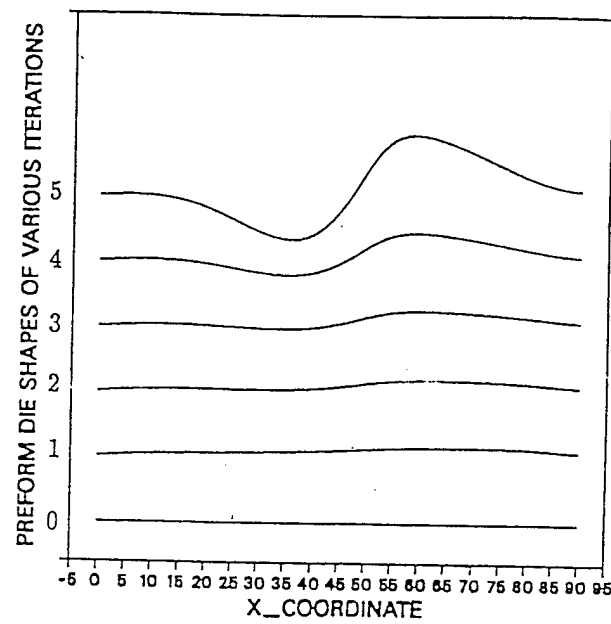


Fig 13. Iteration history of the preform die shapes in axisymmetric deformation.